

Monitoring Atlantic overturning circulation and transport variability with GRACE-type ocean bottom pressure observations - a sensitivity study

Katrin Bentel¹, Felix W. Landerer¹, and Carmen Boening¹

¹Jet Propulsion Laboratory, California Institute of Technology

Correspondence to: Katrin Bentel (Katrin.I.Bentel@jpl.nasa.gov)

Abstract. The Atlantic Meridional Overturning Circulation (AMOC) is a key mechanism for large-scale northward heat transport and thus plays an important role for global climate. Relatively warm water is transported northward in the upper layers of the North Atlantic Ocean, and after cooling at subpolar latitudes, sinks down and is transported back south in the deeper limb of the AMOC.

5 The utility of in-situ ocean bottom pressure (OBP) observations to infer AMOC changes at single latitudes has been characterized in recent literature using output from ocean models. We extend the analysis and examine the utility of space-based observations of time-variable gravity and the inversion for ocean bottom pressure to monitor AMOC changes and variability between 20°N and 60°N. Consistent with previous results, we find a strong correlation between the AMOC signal and
10 OBP variations, mainly along the western slope of the Atlantic basin. We then use synthetic OBP data - smoothed and filtered to resemble the resolution of the GRACE (**Gravity Recovery and Climate Experiment**) gravity mission, **but without errors** - and reconstruct geostrophic AMOC transport. Due to the coarse resolution of GRACE-like OBP fields, we find that leakage of signal across the step slopes of the ocean basin is a significant challenge at certain latitudes. **Transport signal RMS are in a
15 similar order of magnitude as error RMS for the reconstructed time series.** However, the interannual AMOC anomaly time series can be recovered from 20 years of monthly GRACE-like OBP fields with errors less than 1 Sverdrup **in many locations.**

1 Introduction

Changes of the Atlantic Meridional Overturning Circulation (AMOC) and associated pole-ward
20 ocean heat transport from the equatorial regions influence climate at higher latitudes significantly. **It has** potentially significant impacts in particular for the Northern Hemisphere as well as Northwest Europe's climate (Manabe and Stouffer (1999), Srokosz et al. (2012), IPCC (2014)). The dynamics of the mean and time-variable North Atlantic MOC (**Meridional Overturning Circulation**) have been described in several recent studies, using observations from hydrographic arrays such as RAPID-
25 MOCHA (**MOCHA - Meridional Overturning Circulation and Heatflux Array**), e.g., Kanzow et al.

(2010); Elipot et al. (2013), and MOVE (**Meridional Overturning Variability Experiment**), Send et al. (2011), as well as model studies (e.g., Vellinga and Wood (2002), Bingham and Hughes (2008), Bingham and Hughes (2009a), McCarthy et al. (2012), Wunsch and Heimbach (2013)).

30 AMOC variability manifests itself in ocean bottom pressure (OBP) changes, in particular along the western boundary (e.g., Roussenov et al. (2008), Bingham and Hughes (2008), Bingham and Hughes (2012)), but also in in sea surface height changes (e.g., Bingham and Hughes (2009b), Willis (2010), Frajka-Williams (2015)) and in sea surface temperatures (Knight et al. (2005), Zhang (2008)). The viability of using OBP along the eastern and western boundaries to calculate the basin-wide meridional geostrophic transports was first demonstrated with numerical ocean simulations (e.g., Bingham and Hughes (2008), Bingham and Hughes (2009a)). More recently, Elipot et al. (2013) used bottom pressure recorder (BPR) measurements along the western boundary to monitor the AMOC. However, due to the inherent drift problems of in-situ BPR recorders, their analysis was limited to time scales shorter than one year, as well as to the specific latitude of instrument deployment.

40

In the present study, we build upon previous results (Roussenov et al. (2008), Bingham and Hughes (2008), Bingham and Hughes (2009a)) and examine the feasibility of using OBP to derive AMOC variations. While the previous works examined the relationships between OBP and AMOC variability in the North Atlantic at specific latitudes (e.g., 40°N, 48°N and 50°N), we examine the entire latitude and depth range from 20°N through 60°N. Thereby, we specifically investigate the detectability of AMOC variability using OBP inferred from time-variable gravity observations such as those provided by the GRACE satellites (Tapley et al. (2004)). The GRACE gravity observations provide complete global spatial coverage and monthly time series of ocean mass changes from 2002 until present. The challenge in using GRACE-OBP to derive AMOC variability is the relatively coarse spatial resolution as well as overall signal-to-noise levels. To estimate the effects of limited spatial resolution, we use data from the ECCO2 ocean state estimate and convert the synthetic OBP fields to a GRACE-like resolution. To also capture signal contamination from nearby land hydrology variations (which are also recorded by GRACE), we evaluate the effects of terrestrial land water storage on GRACE-like OBP retrievals by combining the ocean state estimate with a land-hydrology model. Our results indicate that even though resolution along the steep basin slopes is challenging in GRACE-like OBP fields, we find that the recovery of the meridional volume transports with errors less than +/-1 Sv is possible for specific regions and time scales.

55

Our paper is organized as follows: in Sect. 2, we briefly review the pertinent aspects of the underlying theories and relationships between OBP and AMOC transports; then we describe the ocean state estimate ECCO2 and discuss the AMOC and OBP signals in the model at GRACE-like spatial resolution, including signal contamination effects from land hydrology; in Sect. 3 we present

60

results for deriving AMOC from the model data directly compared to results for AMOC from data smoothed to a GRACE-like resolution.

65 2 Methods and data

2.1 Theoretical background

The Atlantic meridional overturning circulation consists of a northward flow in the upper layer of the ocean (mostly between the surface and 1000 m depth; Srokosz et al. (2012), Wunsch and Heimbach (2013)), and a return flow to the south in the deeper layer of the ocean (between approximately 1000
70 m to 5000 m depth). The meridional stream function $\psi(y, x)$ is derived from meridional velocities (v_y) by integration over longitudes (x) and from the surface (η) to depth (z) (Marotzke et al. (1999)),

$$\psi(y, z) = \int_W^E \int_z^\eta v_y dz dx. \quad (1)$$

As the large-scale flows are dominated by a geostrophic balance, the meridional transport-per-unit-
75 depth $T(z)$, at a particular latitude (y) and depth (z), can be derived from the zonal bottom pressure differences p_E and p_W at the eastern and western basin boundaries by taking

$$T(z) = \frac{p_E(z) - p_W(z)}{\rho_0 f}, \quad (2)$$

where the constants are the Coriolis parameter f and the mean sea water density ρ_0 (Marotzke et al. (1999), Roussenov et al. (2008)). Acceleration and stress terms are neglected, as they only play a role
80 in the Ekman layer and in the deep bottom layers. For a more rigorous derivation and justification for Eq. 2 we defer to Bingham and Hughes (2008), Bingham and Hughes (2009a), and Roussenov et al. (2008), and references therein. Using the geostrophic approximation, the depth-integrated meridional transports $T(z)$ at a particular latitude (y) can then be used to give the meridional stream function ψ at that latitude:

$$85 \quad \psi(y, \Delta z) = \frac{1}{\rho_0 f} \int_{z_1}^{z_2} (p_E - p_W) dz. \quad (3)$$

Equation 3 provides a method to derive the geostrophic component of the AMOC stream function (or volume transport between two layers) from ocean bottom pressure data along the boundaries of the ocean basin. Possibly intervening topography (i.e., mid-ocean ridges) should in theory be considered when evaluating Eq. 3, but Bingham and Hughes (2008) and Bingham and Hughes (2009a)
90 demonstrated in an ocean model that for interannual time-variable transports in the North Atlantic, bottom pressure variability is concentrated along the western boundary, and it is sufficient to use only the outermost eastern and western points across the basin section (if a basin-mean or depth averaged

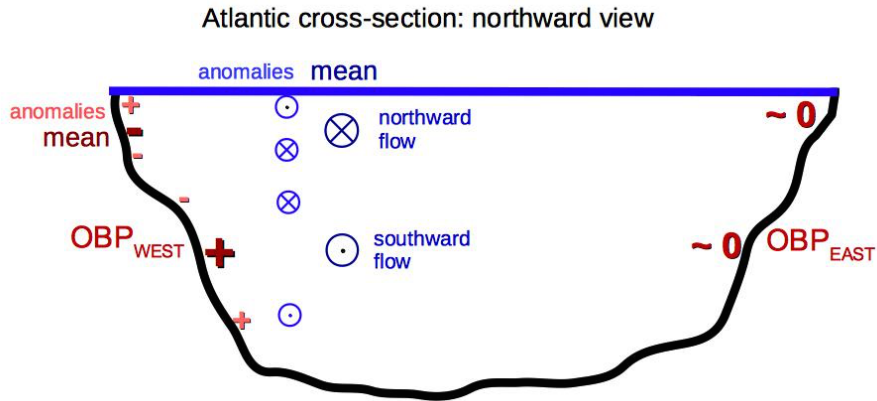


Figure 1. Cross-section of the North Atlantic with an illustration of north- and southward flow temporal mean and anomalies (blue) and associated ocean bottom pressure mean and anomalies (red) along the basin boundaries. Note that in the actual ocean, the bottom pressure signals are largest along the western boundary and the bottom pressure at the eastern boundary is very small and can be neglected. Ocean bottom pressure anomalies are observable with satellite gravimetry

boundary pressure is removed from p_W in Eq. 3, it is also possible to use only bottom pressure on the western boundary (Bingham and Hughes (2009a)). Furthermore, the dominance of the western boundary variations was recently confirmed from hydrographic in-situ data (Elipot et al. (2014)).

95 We reconfirmed this with the ocean model ECCO2 (see below for details), and thus use p_E and p_W only for our analyses in the North Atlantic. While knowledge of p_E and p_W along the boundaries is in principle sufficient to infer $\psi(y, z)$, the actual measurement of these terms is challenging. In-situ BPRs suffer from notorious drift-problems, and thus require drift corrections that usually inhibit any

100 inferences about longer-than-annual variations (Polster et al. (2009)). An alternative measurement of OBP variations can be obtained from time-variable gravity observations from space as currently acquired by the GRACE satellites. The main challenge for OBP inferred from time-variable gravity is the limited horizontal resolution, as well as the required signal sensitivity. Due to the altitude (about 450 km) and orbit configuration of the two GRACE satellites, the horizontal spatial resolution is

105 limited to approximately 300 km (e.g., Chambers and Bonin (2012), Landerer and Swenson (2012)). Much of the AMOC-related OBP signals occur along the narrow and steep western boundary slope and are thus difficult to resolve (which is also a limitation to in-situ pressure observations). In Sect. 3, we therefore quantify these resolution issues using synthetic data at GRACE-like spatial resolutions to quantify the feasibility of the OBP-AMOC approach. Also note that GRACE can only resolve

110 OBP variations relative to a (arbitrary) time-mean. Therefore, all terms in Eqs. 1 - 3 are taken to be anomalies and therefore only AMOC variations can be inferred, but not its long-term average. The mean flow in the North Atlantic and the resulting OBP anomalies are illustrated in Fig. 1.

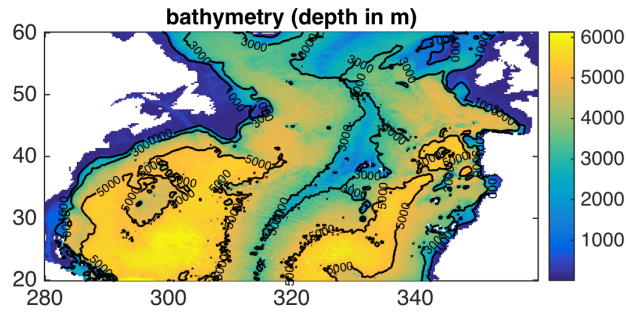


Figure 2. Bathymetry for the North Atlantic with the 1000, 3000, and 5000 m depth contour lines

2.2 Synthetic OBP observations

We use the Estimating the Circulation and Climate of the Ocean, Phase II (ECCO2, Menemenlis et al. (2008)) to reconstruct the AMOC variability from simulated OBP observations in the North Atlantic as in Eq. 3. **ECCO2 is an ocean state estimate which optimally fits ocean observations using a Green’s function approach.** The OBP-derived AMOC reconstructions are compared against the model baseline AMOC, which represents the model truth and is based on the meridional velocities according to Eq. 1. Similar to Bingham and Hughes (2008), we extract zonal OBP profiles following the model’s bathymetry, and then interpolate these values to regularly spaced 100 m depth intervals. Monthly ECCO2-OBP data at a horizontal resolution of 0.25° are computed for the time period January 1993 through December 2012, for the area of the North Atlantic, 80°W to 0°W and 20°N to 60°N . We remove a global mean OBP term to enforce mass conservation (Greatbatch (1994)). For the subsequent analysis, we removed a trend and the mean annual climatology signal from all time series (OBP, velocities), and smooth with a 15-month running mean to focus on interannual signals only.

2.3 GRACE-like OBP fields: mascons and spherical harmonics

Conventional GRACE gravity field solutions are given in global spherical harmonic basis functions without any type of constraints (e.g., Chambers and Bonin (2012)). In contrast, the GRACE mascon solutions employ geophysical constraints, and provide an improved spatial localization. A best-fitting gravity value is estimated for each mascon cell (here: $3^\circ \times 3^\circ$ equal area cells). Importantly, the mascon solution makes the application of empirical post-processing filters (i.e.: destriping) unnecessary and thus features a better signal-to-noise ratio at smaller spatial scales.

We evaluate OBP output from the ECCO2 ocean state estimate as provided at a 0.25° degree resolution. To create GRACE-like synthetic observations that match actual GRACE resolution, we bin-average the OBP fields to a 3 degree equal area grid. This grid is identical to the JPL-mascon RL05M grid (Watkins et al. (2015)). Second, the OBP data is smoothed to resemble the resolution of the

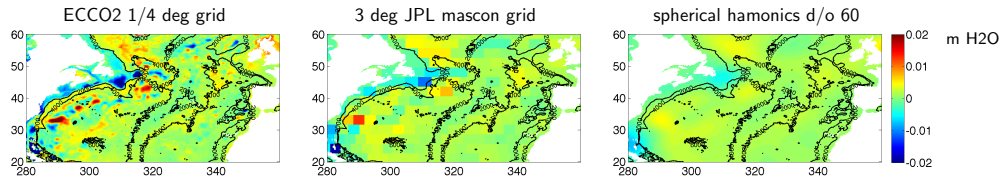


Figure 3. OBP snapshots for January 2012 for the different simulated OBP observation time series: left: 0.25° ECCO2 resolution; center: GRACE JPL mascon resolution (approx. 3 deg); right: GRACE spherical harmonic resolution to spherical harmonic degree 60, smoothed with a 300 km Gaussian filter

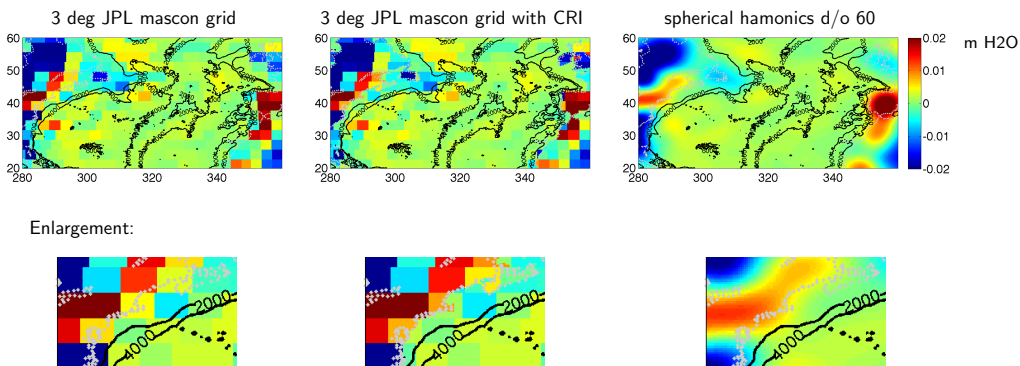


Figure 4. OBP snapshots for January 2012 for the simulated observations, including the continental hydrology signal: left: JPL mascon grid without CRI (coastline resolution improvement); center: JPL mascon grid with CRI, right: spherical harmonics to degree 60. Since the ECCO2 original data is not smoothed, the OBP pixels do not get affected by nearby land hydrology signals (therefore no additional plot for hydrology). Second row shows enlargements of the two mascon-resolution data sets including hydrology and details for CRI

standard GRACE solutions, which are represented in spherical harmonics truncated at degree and order 60, and smoothed with a Gaussian filter with 300 km radius. **This would be necessary for real**

140 **GRACE data in order to reduce noise and correlated errors.** This processing provides approximately the resolution that is currently achieved with the GRACE satellites. However, we do not consider instrument and resulting measurement errors in the gravity field retrieval from GRACE measurements in order to focus on the issues of spatial resolution and signal leakage. The spatial smoothing and averaging of the 0.25° OBP fields leads to significant resolution reduction in particular in highly energetic regions like the Gulf Stream, as well as in regions of steep bathymetry (Fig. 2, Fig. 3).

145 **Additional post-processing filters employed to reduce correlated errors in GRACE would further dampen geophysical signals (e.g., Landerer and Swenson (2012)).**

2.4 Leakage effects

2.4.1 From continental hydrology

150 In order to make the synthetic OBP observations more realistic, we add a continental hydrology signal that we obtain from the GLDAS-NOAH hydrology model (Rodell et al. (2004)). The continental hydrology signal does not affect the OBP data on the 0.25° ECCO2 grid. However, when the data is smoothed, the hydrology signal 'leaks' into the OBP data (Wahr et al. (1998), Chambers and Bonin (2012)), causing **contamination** of ocean grid points by land hydrology variations (Fig. 4). As the
155 following analysis will show, the effects of land signal leakage tend to dominate the error budget in the meridional transport and overturning calculations, in particular for the near-coastal shallower shelf areas (above approx. 1000 m). Therefore, a leakage correction (e.g., CRI (**coastline resolution improvement**) filter for the mascon-grid) is essential in order to employ GRACE OBP-observations: mascons that cover both land and ocean area still obtain only one value to represent the mass change
160 within that mascon. To better distinguish where the signals originate from, a so-called coastline resolution improvement (CRI) filter is employed (see Watkins et al. (2015) for details). Essentially, the CRI process separates land hydrology and ocean signals based on a-priori co-variance information from both land and ocean forward simulations. This CRI filter reduces the leakage of the continental hydrology signal into the adjacent ocean mascons significantly (Fig. 4).
165 **Spherical harmonic GRACE solutions can be corrected for leakage as well, using an iterative approach. However, due to large smoothing filters which need to be applied (300 km Gaussian smoothing radius) and errors in the hydrology models, these corrections are not sufficient enough to reduce overall noise and errors in the solutions for our purposes. We therefore do not consider leakage correction for spherical harmonics further here.**

170 2.4.2 Due to steep bathymetry gradients

Besides signal leakage from continental hydrology, leakage of the signal within the ocean between different depths must be considered. Especially along the steep basin boundary slopes, there are instances where one 3 degree mascon covers a number of different depth layers. Thus, the different OBP in these layers cannot be resolved. One possibility to make this leakage effect smaller is optimal
175 placement in longitude of the individual mascon cells. In the JPL mascon grid, it is possible to shift the mascons in longitude direction (for each mascon latitude) without influencing mascons in other latitudes. We create a synthetic data set where we position the JPL mascons optimally in order to resolve as much of the western and eastern boundary signal as possible.

Table 1. Overview of the different resolutions of the synthetic OBP data

Acronym	Characteristics	Spatial resolution
T^O	Original ECCO2 OBP grid	0.25°
T^{SH60}	Spherical harmonic expansion up to d/o 60, smoothed with a Gaussian filter of 300 km radius and synthesized back to a point grid	3°
T^{MSC}	Interpolated to approx. 3° equal area JPL mascon grid, which is described in Watkins et al. (2015)	3°
$T^{MSC+CRI}$	Interpolated to approx. 3° equal area JPL mascon grid, and CRI (coastline resolution improvement) applied (Watkins et al. (2015))	3°
$T^{MSC+POSOPT}$	Interpolated to a grid similar to the JPL mascon grid, with the grid cells' longitude position adjusted to minimized RMS error (minimizing leakage over different depths and land hydrology leakage simultaneously)	3°

3 Results

180 Equation 3 is evaluated for different synthetic OBP resolutions derived from ECCO2 in the North Atlantic: the original ECCO2 0.25° grid (T^O), a GRACE spherical harmonics grid truncated at degree and order 60 (T^{SH60}), GRACE mascon grids, without (T^{MSC}) and with ($T^{MSC+CRI}$) CRI filter, and position optimized mascons ($T^{MSC+POSOPT}$). See Tab. 1 for a summary of the corresponding OBP grid characteristics. The OBP-reconstructed transports are then evaluated against the
185 model baseline transports, which are derived directly from the meridional velocities. While the OBP signal on the western basin boundary contains most of the AMOC information, a basin mode has to be taken into account, either by differencing with the signal on the eastern boundary, or by removing a depth-averaged OBP to remove variations not contributing to geostrophic transports (Bingham and Hughes (2008), Bingham and Hughes (2009a)). Even though the eastern boundary OBP contributes
190 only a small fraction to the AMOC signal, we take the signal on the eastern boundary into account rather than removing a depth-mean. By removing a mean over all depths, leakage signal from continental hydrology would contaminate the OBP data at greater depths as well as the shallower areas, and degrade the AMOC transport estimates compared to the East-West difference. Thus, we consider the eastern boundary in our calculation, even though the data on the eastern boundary reduces the
195 signal-to-noise ratio.

3.1 Meridional transports from OBP integration

For each of the synthetic OBP data sets, meridional transport time series are computed in 1° latitude increments and over 100 m depth intervals, and the RMS differences between reconstructed and model reference time series are computed for each depth and latitude (Fig. 5). The results for
200 OBP without a hydrology signal (Fig. 5, top row) at the 0.25° native ECCO2 resolution leads to

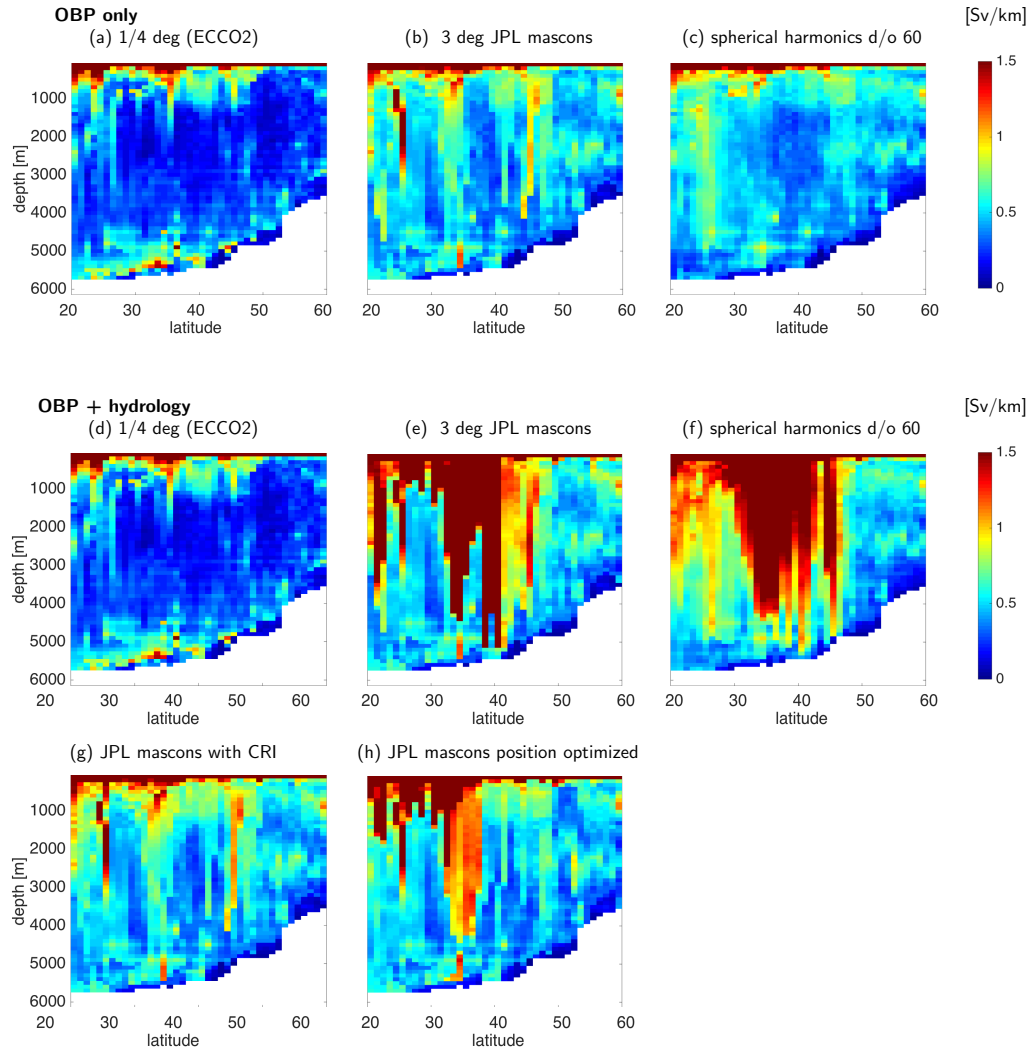


Figure 5. RMS errors for the computed transport-per-unit-depth T in [Sv/km] from eastern and western boundary OBP according to Eq. 3. OBP only (top row) and OBP + hydrology (second and third row) for each of the synthetic observation time series. Significant leakage errors are introduced with the GRACE-like resolutions (second row), CRI filtering of the mascons and optimizing their position in longitude can remove a major part of the leakage errors

errors smaller than 0.5 Sv/km for depths between 1000 and 5000 m. At latitudes lower than 50°N , errors above 1000 and below 5000 m vary with latitude and depend on the bathymetry gradients. At GRACE-like resolutions (panels B and C in Fig. 5), the errors are slightly higher across all depths, and at specific latitudes, e.g., at $25 - 30^\circ\text{N}$, there are significant signal leakage errors that introduce significant transport retrieval errors. **The steep topography (Fig. 2) at these latitudes causes one 3° mascon to cover depth layers from above 1000 m to below 3000 m.** Very high errors (> 1.5 Sv/km) occur in the upper 100 m depth for all latitudes due to the non-geostrophic, wind-driven transport

in the Ekman layer, which cannot be recovered from East-West OBP difference observations. In all following computations of the geostrophic volume transports, we therefore exclude the upper 100 m (in the OBP-derived as well as in the reference transport time series).

While the GLDAS hydrology signal does not affect the results on the ECCO2 model grid (Fig. 5, panel D), significant leakage errors from land hydrology are introduced when the OBP and hydrology signals are spatially smoothed to GRACE-like resolutions (Fig. 5, E and F). Without hydrology leakage, errors of 1.5 Sv/km and larger only occur in the uppermost 100 m when Ekman transports are not accounted for, and at 25°N for the mascons. With hydrology leakage effects, the GRACE-like OBP resolutions lead to high errors that extend into deeper layers, down to 3000 to 5000 m depth for latitudes 32°N to 40°N. This effect is highly latitude-dependent, since the lower resolution only degrades the results if smoothing occurs over too many depth layers and/or the coastline. In this way, the results are very dependent on the bathymetry and the proximity of depth contours to land points, as well as signal amplitudes over land. In addition, pressure variations over steep bathymetry cannot be adequately resolved in the spatially smoothed data. For the mascon resolution, the leakage effect changes with mascon latitudes. Significant hydrology signal leakage occurs especially between 35°N and 40°N, down to a depth of 2000 m. For spherical harmonics, the leakage effects are more smeared out over depths and latitudes. Between 20°N and 40°N down to 3000 m depth errors are between 1 Sv/km and 2 Sv/km. For the mascon results, the CRI filter reduces much of the leakage artefacts; the major leakage effect between 35°N and 40°N is reduced from errors exceeding 2 Sv/km to less than 1 Sv/km by 2000 m depth.

Another strategy to reduce leakage is to optimize the placement of the individual mascons in longitude direction (for each mascon latitude). When mascon boundaries align with the coastline, hydrology leakage is reduced, and when an individual mascon does not cover too many depth layers, leakage between depths in the ocean is reduced. The optimal mascon position (in longitude) is found by minimizing both types of errors simultaneously. While there are latitudes where land leakage is not reduced as much by optimal positioning as by the CRI filter (e.g., 22°N, 33°N), errors in the deeper layers between 2000 m and 3000 m depths are smaller than for the CRI results. For 30°N to 50°N and between 1500 m and 5000 m depth most errors are below 0.5 Sv/km with the position optimized mascons, while they tend to be between 0.5 and 1 Sv/km in the results with CRI. Note that CRI only treats and reduces land-leakage, but does not mitigate leakage between different ocean depths layers (Watkins et al. (2015)).

3.2 Reconstructing north- and southward transports

The maximum of the mean model AMOC in ECCO2 lies at 32°N and 909 m depth, Fig. 6. Thus, net transports from the surface to about 909 m are northward, and net transports below about 909

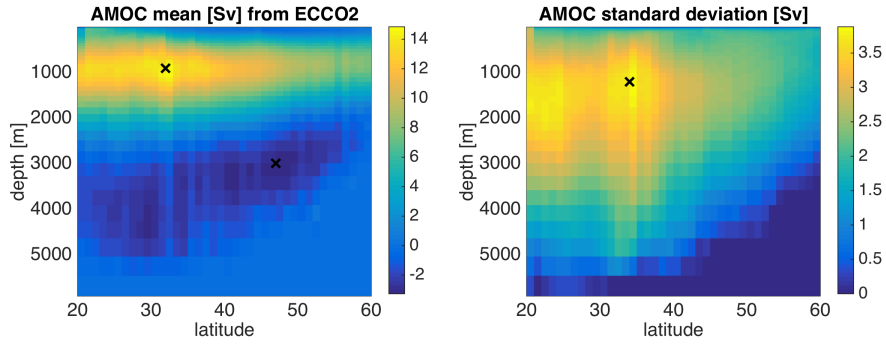


Figure 6. Left panel: Time mean of AMOC from ECCO2, with maximum at 32°N, 909 m depth, minimum at 47°N, 2990 m depth, both indicated marker X, right panel: variability of AMOC from ECCO2, maximum at 34°N, 1200 m depth, indicated by marker X

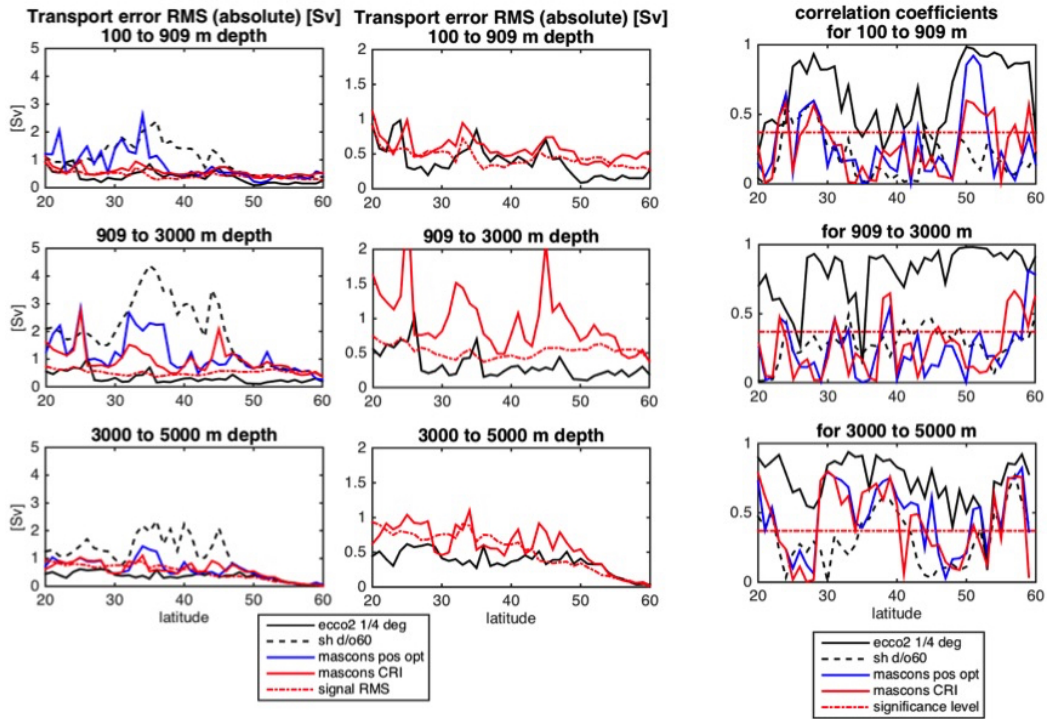


Figure 7. Error RMS and correlation coefficients for reconstructed net transport in three different depth layers and from different OPB resolutions (native ECCO2 grid vs. GRACE-like resolutions). Left: error RMS for the computed time series and RMS signal time series (red dashed); center: selection of two cases of error RMS and different scales on the plots; right: correlation coefficients of the derived time series versus the model truth, red dashed line indicates significance level

m to a depth of about 5000 m southward. **However, the depth of maximum overturning varies with**
245 **latitude and in time.** The circulation below about 5000 m is linked to the Atlantic Bottom Water
and is not considered in the following. As mentioned before, the uppermost 100 m of the ocean are
also excluded, because the Ekman circulation and related transports cannot be recovered from OBP
gradients. Over interannual periods, the net water volume transported northward should equal the
water volume transported back south (e.g., Srokosz et al. (2012), or Kanzow et al. (2007) for 10-day
250 timescales). Thus, it should be sufficient to observe either the northward or the southward transport
in order to reconstruct the interannual AMOC transport variations, **as long as the depth of maximum**
overturning circulation is known. Since we do not know the correct depth of maximum overturning
for each latitude and time, we make an assumption of a constant depth, which introduces only a
small error.

255

In what follows, three different depth layers are considered in more detail: 100 m to 909 m, 909 m
to 3000 m, and 3000 m to 5000 m depth, and detectability of the AMOC signal in each of these three
layers from GRACE-like OBP resolutions is assessed. The first layer covers the northward trans-
port (down to the maximum of the mean AMOC, Fig. 6), the second layer covers steep ocean basin
260 slopes for most latitudes (Fig. 2), and the third layer covers deeper transport, where the bathymetry
is less steep (Fig. 2), and therefore can be expected to be more favorable for GRACE-like resolutions.

Figure 7 shows RMS errors and correlation coefficients for the reconstructed transport versus
the model baseline for the three layers. **The center plot is a selection of the plots on the left, with**
265 **an adjusted axis to enhance details for the solutions with smaller errors (ECCO2 native resolution**
and mascons with CRI). The reconstructed transport from OBP at the ECCO2 native 0.25° resolu-
tion (black curves Fig. 7) matches the model baseline transport best; it shows smallest RMS errors
(about 0.5 Sv and below, with a maximum of 1 Sv) for all the three layers and the highest correlation
coefficients. The average error RMS and correlation level is similar for all the three layers under con-
sideration. However, when smoothing to GRACE-like resolutions, RMS differences become larger
and correlation coefficients smaller, due to the much coarser resolution of 3° . For these resolutions,
overall and maximum RMS errors (Fig. 7, left) are larger for the medium depth layer (909 m to 3000
m) than for the upper and the deep layers. The larger errors between 20°N and 45°N in the medium
layer for data at GRACE-like resolutions are caused by the steep slopes between about 1000 m and
275 3000 m depth (Fig. 2, Fig. 4). When the data is smoothed, the OBP values cannot be attributed to the
correct depth as the depth interval for one 3° smoothing interval becomes very large. Between 45°N
and 60°N , the depth gradient for a 3° longitude interval becomes much smaller, i.e., more than one
three degree pixel is needed to cover the depth gradient from 909 m to 3000 m. Thus, OBP at **indi-**
vidual depth layers can be better resolved and the transport reconstruction is more accurate, leading
280 to smaller error RMS. For the upper transport, RMS errors are high (0.5 Sv to 2 Sv) for spherical

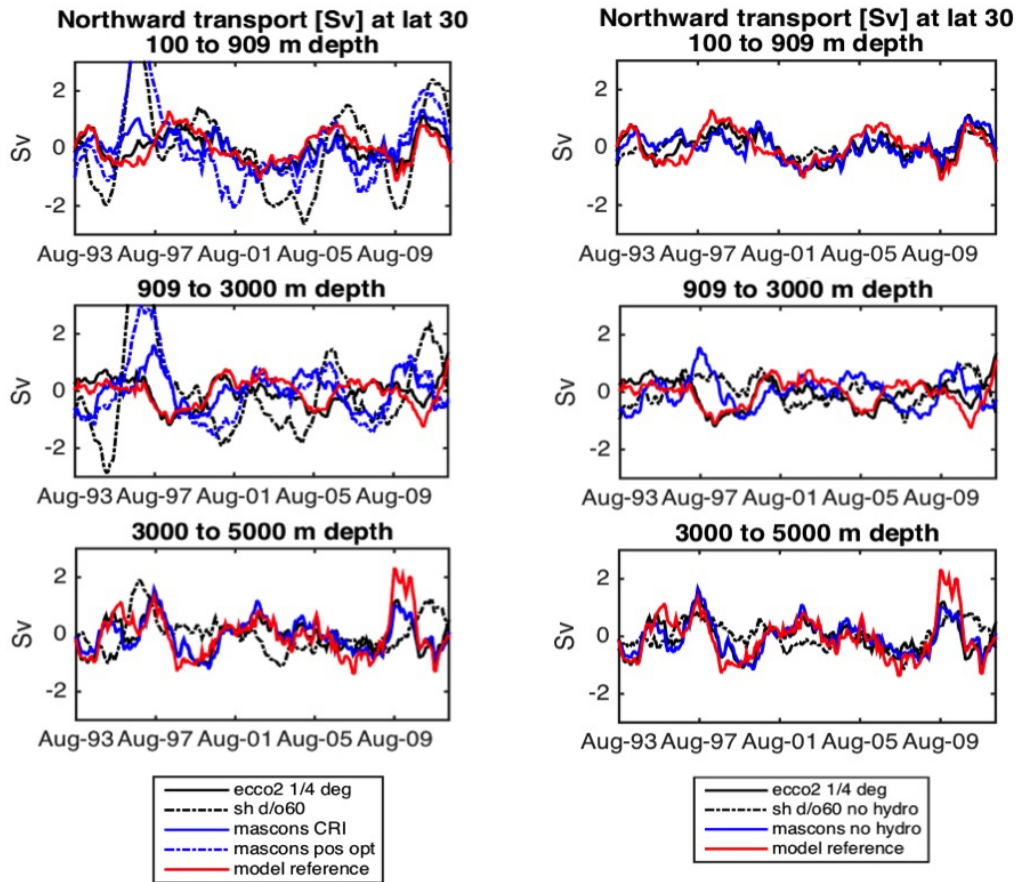


Figure 8. Transport time series anomalies at 30°N , reconstructed from different OBP data sets versus the model baseline, left: including land hydrology signal, right: without land hydrology signal

harmonics and mascons, and especially high between 30°N and 40°N . These errors are attributed to leakage effects from land hydrology signals (Fig. 5). In the upper layer, the coastline resolution improvement correction makes a big difference: For mascons with CRI (red curve in Fig. 7) the error RMS are at a level similar to the ECCO2 native 0.25° resolution and below 1 Sv. In the deep layer (3000 m to 5000 m depth), there are still high error RMS of about 3 Sv between 30°N and 40°N for spherical harmonics (black dashed curve), because land hydrology leakage extends to depths below 3000 m for these latitudes (Fig. 5). The CRI algorithm and position optimizing of mascons corrects for these errors, therefore, error RMS for mascons with CRI and position optimized mascons (red and blue curves) are about and below 1 Sv in the deep layer for 20°N to 45°N . Beyond 45°N , the GRACE resolution is well capable to capture all the OBP signal, since the bathymetry is less steep. Therefore, error RMS decrease, and drop below 0.5 Sv for 50°N to 60°N . In order to show more detail with respect to the signal RMS, the two solutions with smaller error RMS, i.e. the original ECCO2 grid and mascons with CRI, are plotted again in the center of Fig. 7. Even for these better

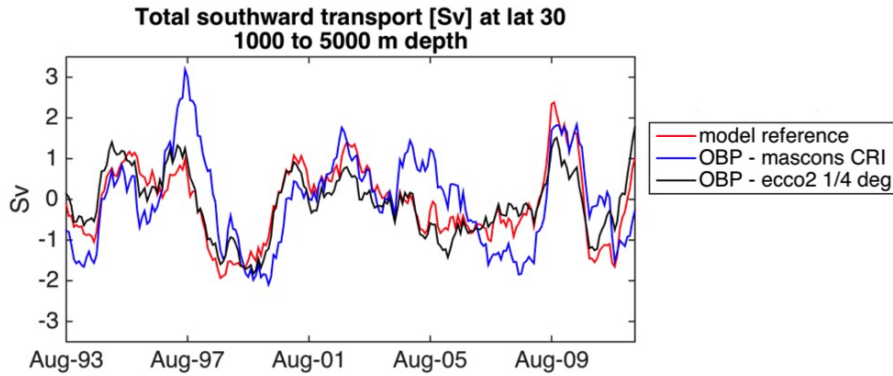


Figure 9. AMOC transport time series anomalies at 30 N; reconstruction from OBP versus model baseline (from velocities); error RMS mascons 0.90 Sv, ECCO2 grid 0.43, correlation coefficient mascons 0.63, ECCO2 grid 0.88

performing solutions, the signal RMS is in the same order of magnitude as the error RMS, with the error RMS from the mascon solutions exceeding the signal RMS by far in the intermediate layer. The errors RMS for the original ECCO2 resolution is mostly just below the signal RMS. Even though error RMS for mascons are higher, the results in the upper and deeper layers achieve smaller error RMS than signal RMS for selected latitudes. As mentioned before, the overturning transport signal is on the edge of detectability in GRACE gravity data, but we show in this study that it is possible with CRI improved mascons for selected latitudes.

Correlation coefficients vary a lot with latitude. While correlation coefficients are highest for the 0.25° ECCO2 resolution, the difference to the GRACE-like resolutions is the largest in the medium layer, due to steep basin boundary in this layer, as explained above. Even though there are a few latitudes with poor correlation in the deep layer for the GRACE-like resolutions (e.g., between 25°N and 30°N, and 40°N to 50°N), the correlation coefficients are overall higher than in the upper two layers, where most correlation coefficients are below 0.5. Most correlation coefficients with the time series from OBP at the original ECCO2 resolution are significant (Fig. 8 black curve above red dashed significance level), while significance of the correlation coefficients varies a lot with latitude for GRACE-like resolutions (all other curves). Especially in the deep layer, there are several latitudes, where correlation coefficients for mascons with CRI are well above the significance level, e.g., 20 - 25N, 30 - 40N, 55 - 60N. Again, this indicates that the less steep bathymetry in the deep layer is more favorable for GRACE-like resolutions.

In conclusion, Fig. 7 shows that the upper and the deep layer transport can be reconstructed from GRACE-like OBP resolutions with error RMS of 0.5 Sv and correlation coefficients of about 0.7, as long as leakage from land hydrology is accounted and corrected for. The medium layer (909 m to

3000 m depth) is much less suitable for transport reconstruction from GRACE-like OBP resolutions, because the steep bathymetry in this layer cannot be resolved well by GRACE.

320

Fig. 8 shows one example for reconstructed transport time series at 30°N. The left hand side of the figure shows the results for OBP time series including continental hydrology, while the right hand side shows the corresponding time series, but for the OBP signal only, without hydrology. The magnitude of the model reference signal which we are trying to recover is about the same for the upper and the intermediate layer (well below 2 Sv), but it reaches and exceeds 2 Sv in some months for the deep layer. In the upper and intermediate layer, there is a very large signal magnitude in the time series derived from spherical harmonics and position optimized mascons including land hydrology. This large signal magnitude is caused by leakage of the continental hydrology signal (larger magnitude than OBP signal). It is not present in the solution without hydrology. Also note that leakage affects even the intermediate depth layer at this latitude, i.e. below 909 m depth. The original ECCO2 grid is not affected by hydrology, therefore the solid black curves are the same in the plots on the right and on the left. Leakage from continental hydrology does not affect the very deep layers, thus, the results on the right and on the left for the deep layer are the same. Without any leakage, reconstruction of the transport signal works well for all different OBP time series for the upper layer. However, this scenario is not very realistic. Even though a good portion of the signal can be recovered, the solution from spherical harmonics show the largest discrepancies from the model reference for the scenario without hydrology. From the mascon resolution, the signal can be recovered well in the deep layer, however, there are some discrepancies in the intermediate layer which are due to signal leakage across different depth due to steep bathymetry. In conclusion, first and foremost, continental hydrology has to be taken into account, for example with the CRI filter for the mascons. Second, leakage across steep bathymetry contaminates the transport signal derived from mascon-resolution OBP. Favorable latitudes and depth layers for less steep bathymetry gradients have to be chosen.

345 Finally, Fig. 9 shows our AMOC reconstruction for 30°N, derived by summing up the time series for the intermediate and the deep transport layer, i.e. showing the total southward transport (which we assume to be compensating to the entire AMOC northward transport). The model reference time series is matched closely by the time series derived from OBP at the original ECCO2 grid. There are some larger discrepancies between the model reference and the time series derived from mascons (with CRI), blue curve in Fig. 9. Nevertheless, the model reference can be recovered with an error RMS of 0.90 SV and a correlation coefficient of 0.63. While in the deep layer transport (bottom panel, left, in Fig. 8), the time series derived from mascons with CRI and the original ECCO2 grid are very similar (black and blue solid curves), they differ for the intermediate layer, while the black curve (ECCO2 grid) is closer to the model reference. This is what introduces errors to the mascon

350

355 time series in Fig. 9. While the CRI takes care of continental hydrology leakage, there is leakage
across the steep bathymetry at depths between 909 and 3000 m (compare solid blue curves left and
right hand side, intermediate panel in Fig. 8).

4 Summary and outlook

Our model studies have shown that even though signal leakage (from hydrology and across different
360 depths layers) is a challenge at GRACE-like resolutions, the AMOC anomaly time series can be
retrieved from GRACE-like OBP observations with errors of +/-1 Sv and below. (This is of similar
accuracy as for the full time variable AMOC recovery by RAPID (McCarthy et al. (2015))). The
AMOC retrieval is rather sensitive to the bathymetry profile, and therefore the quality of the signal
recovery is very latitude dependent (Fig. 7, errors vary with latitude and depth layer from 0.05 Sv
365 to 5 Sv). Furthermore, error RMS levels are in the same order of magnitude as signal RMS levels
(Fig. 7); they are smaller only for selected depths and latitudes. However, in the deeper layers of the
ocean (where the bathymetry gradients are less steep than in shallower layers), OBP measurements at
GRACE-like resolutions lead to errors below 1 Sv, while they are up to 3 Sv for the other two layers
(Fig. 7). Thus, the deep layer appears to be the most suitable target to retrieve ocean transports
370 from OBP observations at GRACE-like resolutions. Since the AMOC is not very coherent with
latitude and OBP recorder measurements suffer from drift over longer periods of time, satellite
gravity measurements (GRACE-like OBP) present a unique dataset to monitor AMOC changes over
large areas (like the whole North Atlantic basin) and over extended periods of time (GRACE time
series span from 2002 up to today). Our next steps and ongoing work are to move from model
375 simulations to real data and use the OBP integration analysis on JPL5M GRACE mascons to derive
real AMOC anomaly time series from the satellite-based OBP observations.

Acknowledgements. The research described in this paper was carried out at the Jet Propulsion Laboratory, Cal-
ifornia Institute of Technology, sponsored by the National Aeronautics and Space Administration (NASA), and
with support from the NASA Physical Oceanography program.

380

Copyright 2015 California Institute of Technology. U.S. Government sponsorship acknowledged.

References

- Bingham, R. J. and Hughes, C. W.: Determining North Atlantic meridional transport variability from pressure on the western boundary: A model investigation, *J. Geophys. Res.*, 113, doi:10.1029/2007JC004679, 2008.
- 385 Bingham, R. J. and Hughes, C. W.: Geostrophic dynamics of meridional transport variability in the subpolar North Atlantic, *J. Geophys. Res.*, 114, C12 029, doi:10.1029/2009JC005492, 2009a.
- Bingham, R. J. and Hughes, C. W.: Signature of the Atlantic meridional overturning circulation in sea level along the east coast of North America, *Geophys. Res. Lett.*, 36, 2009b.
- Bingham, R. J. and Hughes, C. W.: Local diagnostics to estimate density-induced sea level variations over
390 topography and along coastlines, *J. Geophys. Res.*, 117, 2012.
- Chambers, D. P. and Bonin, J. A.: Evaluation of Release-05 GRACE time-variable gravity coefficients over the ocean, *Ocean Sci.*, 8, 859–868, doi:10.5194/os-8-859-2012, 2012.
- Elipot, S., Frajka-Williams, E., Hughes, C. W., and Willis, J. K.: The Observed North Atlantic Meridional Overturning Circulation: Its Meridional Coherence and Ocean Bottom Pressure, *J. Phys. Oceanogr.*, 44,
395 517–537, doi:10.1175/JPO-D-13-026.1, <http://dx.doi.org/10.1175/JPO-D-13-026.1>, 2013.
- Elipot, S., Frajka-Williams, E., Hughes, C. W., and Willis, J. K.: The Observed North Atlantic Meridional Overturning Circulation: Its Meridional Coherence and Ocean Bottom Pressure, *J. Phys. Oceanogr.*, 44,
517–537, doi:10.1175/JPO-D-13-026.1, <http://dx.doi.org/10.1175/JPO-D-13-026.1>, 2014.
- Frajka-Williams, E.: Estimating the Atlantic overturning at 26°N using satellite altimetry and cable measure-
400 ments, *Geophys. Res. Lett.*, 42, 3458–3464, doi:10.1002/2015GL063220, 2015.
- Greatbatch, R. J.: A note on the representation of steric sea level in models that conserve volume rather than mass, *J. Geophys. Res.*, 99, 12,767 – 12,771, 1994.
- IPCC: Climate Change 2014: Impacts, Adaptation, and Vulnerability. Part A: Global and Sectoral Aspects. Contribution of Working Group II to the Fifth Assessment Report of the Intergovernmental Panel on Climate
405 Change (Field, C.B., V.R. Barros, D.J. Dokken, K.J.), 2014.
- Kanzow, T., Cunningham, S. A., Rayner, D., Hirschi, J. J.-M., Johns, W. E., Baringer, M. O., Bryden, H. L., Beal, L. M., Meinen, C. S., and Marotzke, J.: Observed Flow Compensation Associated with the MOC at 26.5°N in the Atlantic, *Science*, 317, 938–941, doi:10.1126/science.1141293, 2007.
- Kanzow, T., Cunningham, S. a., Johns, W. E., Hirschi, J. J.-M., Marotzke, J., Baringer, M. O., Meinen, C. S.,
410 Chidichimo, M. P., Atkinson, C., Beal, L. M., Bryden, H. L., and Collins, J.: Seasonal Variability of the Atlantic Meridional Overturning Circulation at 26.5°N, *J. Clim.*, 23, 5678–5698, doi:10.1175/2010JCLI3389.1, 2010.
- Knight, J. R., Allan, R. J., Folland, C. K., Vellinga, M., and Mann, M. E.: A signature of persistent natural thermohaline circulation cycles in observed climate, *Geophys. Res. Lett.*, 32, doi:10.1029/2005GL024233,
415 2005.
- Landerer, F. W. and Swenson, S. C.: Accuracy of scaled GRACE terrestrial water storage estimates, *Water Resour. Res.*, 48, doi:10.1029/2011WR011453, 2012.
- Manabe, S. and Stouffer, R. J.: The role of thermohaline circulation in climate, *Tellus B*, 51, 91–109, doi:10.1034/j.1600-0889.1999.00008.x, 1999.

- 420 Marotzke, J., Giering, R., Zhang, K. Q., Stammer, D., Hill, C., and Lee, T.: Construction of the adjoint MIT ocean general circulation model and application to Atlantic heat transport sensitivity, *J. Geophys. Res. Ocean.*, 104, 29 529–29 547, doi:10.1029/1999JC900236, 1999.
- McCarthy, G., Frajka-Williams, E., Johns, W. E., Baringer, M. O., Meinen, C. S., Bryden, H. L., Rayner, D., Duce, R. A., Roberts, C., and Cunningham, S. a.: Observed interannual variability of the Atlantic meridional overturning circulation at 26.5°N, *Geophys. Res. Lett.*, 39, doi:10.1029/2012GL052933, 2012.
- 425 McCarthy, G., Smeed, D., Johns, W., Frajka-Williams, E., Moat, B., Rayner, D., Baringer, M., Meinen, C., Collins, J., and Bryden, H.: Measuring the Atlantic Meridional Overturning Circulation at 26°N, *Prog. Oceanogr.*, 130, 91–111, doi:10.1016/j.pocean.2014.10.006, 2015.
- Menemenlis, D., Campin, J.-M., Heimbach, P., Hill, C., Lee, T., Nguyen, A., Schodlok, M., and Zhang, H.: ECCO2: High Resolution Global Ocean and Sea Ice Data Synthesis, *Mercat. Ocean Q. Newsl.*, p. 13, 2008.
- 430 Polster, A., Fabian, M., and Villinger, H.: Effective resolution and drift of parascientific pressure sensors derived from long-term seafloor measurements, *Geochemistry, Geophys. Geosystems*, 10, doi:10.1029/2009GC002532, 2009.
- Rodell, M., Houser, P. R., Jambor, U., Gottschalck, J., Mitchell, K., Meng, C.-J., Arsenault, K., Cosgrove, B., Radakovich, J., Bosilovich, M., Entin, J. K., Walker, J. P., Lohmann, D., and Toll, D.: The Global Land Data Assimilation System, *Bull. Am. Meteorol. Soc.*, 85, 381–394, doi:10.1175/BAMS-85-3-381, 2004.
- 435 Roussenov, V. M., Williams, R. G., Hughes, C. W., and Bingham, R. J.: Boundary wave communication of bottom pressure and overturning changes for the North Atlantic, *J. Geophys. Res.*, 113, doi:10.1029/2007JC004501, 2008.
- 440 Send, U., Lankhorst, M., and Kanzow, T.: Observation of decadal change in the Atlantic meridional overturning circulation using 10 years of continuous transport data, *Geophys. Res. Lett.*, 38, 1–5, doi:10.1029/2011GL049801, 2011.
- Srokosz, M., Baringer, M., Bryden, H., Cunningham, S., Delworth, T., Lozier, S., Marotzke, J., and Sutton, R.: Past, present, and future changes in the atlantic meridional overturning circulation, *Bull. Am. Meteorol. Soc.*, 93, 1663–1676, doi:10.1175/BAMS-D-11-00151.1, 2012.
- 445 Tapley, B. D., Bettadpur, S., Ries, J. C., Thompson, P. F., and Watkins, M. M.: GRACE Measurements of Mass Variability in the Earth System, *Sci.*, 305, 503–505, doi:10.1126/science.1099192, 2004.
- Vellinga, M. and Wood, R. A.: Global Climatic Impacts of a Collapse of the Atlantic Thermohaline Circulation, *Clim. Change*, 54, 251–267, 2002.
- 450 Wahr, J., Molenaar, M., and Bryan, F.: Time variability of the Earth's gravity field: Hydrological and oceanic effects and their possible detection using GRACE, *J. Geophys. Res.*, 103, 205–229, doi:10.1029/98JB02844, 1998.
- Watkins, M. M., Wiese, D. N., Yuan, D.-N., Boening, C., and Landerer, F. W.: Improved methods for observing Earth's time variable mass distribution with GRACE using spherical cap mascons, *J. Geophys. Res. Solid Earth*, 120, doi:10.1002/2014JB011547, 2015.
- 455 Willis, J. K.: Can in situ floats and satellite altimeters detect long-term changes in Atlantic Ocean overturning?, *Geophys. Res. Lett.*, 37, doi:10.1029/2010GL042372, 2010.

- Wunsch, C. and Heimbach, P.: Two decades of the atlantic meridional overturning circulation: Anatomy, variations, extremes, prediction, and overcoming its limitations, *J. Clim.*, 26, 7167–7186, doi:10.1175/JCLI-D-12-00478.1, 2013.
- 460
- Zhang, R.: Coherent surface-subsurface fingerprint of the Atlantic meridional overturning circulation, *Geophys. Res. Lett.*, 35, 1–6, doi:10.1029/2008GL035463, 2008.